Available online at www.sciencedirect.com
ScienceDirect
Advances in Space Research 42 (2008) 844–851
ADVANCES IN SPACE RESEARCH (a COSPAR publication)
www.elsevier.com/locate/asr

Gradient pattern analysis of short solar radio bursts

R.R. Rosa [a,*], M. Karlický [b], T.B. Veronese [a], N.L. Vijaykumar [a], H.S. Sawant [c], A.I. Borgazzi [d], M.S. Dantas [a], E.B.M. Barbosa [a], R.A. Sych [e], O. Mendes [d]

[a] *Laboratório Associado de Computação e Matemática Aplicada (LAC), Instituto Nacional de Pesquisas Espaciais (INPE) São José dos Campos – São Paulo, Brazil*
[b] *Astronomical Institute of Academy of Sciences of the Czech Republic, Ondrejov, Czech Republic*
[c] *Divisão de Astrofísica (DAS) – INPE, Brazil*
[d] *Divisão de Geofísica Espacial (DGE) – INPE, Brazil*
[e] *Institute of Solar-Terrestrial Physics, Irkutsk, Russia*

Received 7 November 2006; received in revised form 20 July 2007; accepted 14 August 2007

Abstract

We analyze the weak component of the localized temporal pattern variability of 3 GHz solar burst observed by the *Ondrejov radio-spectrograph*. A complex, short and weak impulsive sample from the time series was analyzed by applying a method based on the gradient pattern analysis and discrete wavelet decomposition. By analyzing canonical temporal variability patterns we show that the new method can reliably characterize the phenomenological dynamical process of short time series ($N \leqslant 10^3$ measurements) as the radio burst addressed here. In the narrowest sense, by estimating the mutual information distance in the gradient spectra, we show that the fluctuation pattern of the short and weak 3 GHz impulsive solar burst, with energetic amplitudes <350 SFU, is closer to the intermittent and strong MHD turbulent variability pattern.

Keywords: Solar radio bursts; Stochastic processes; Gradient pattern analysis; Wavelets; MHD turbulence

1. Introduction

Solar flares frequently radiate in the lowest microwave range (1–3 GHz) but not much is known about the complex pattern variability of these emissions. However, it is known that the large amount of energy released during a solar flare and the relatively short timescale in which all related events occur lead to the conclusion that a solar flare is a magneto-hydrodynamic (MHD) instability taking place in a strongly anisotropic turbulent plasma (Kuperus, 1976). In this context, the solar radio burst at 3 GHz observed during the June 6, 2000 flare, has been analyzed for its complex temporal variability, which was also observed by EIT/SOHO and SXT/Yohkoh, whose images indicate the complex spatio-temporal flare loop interactions. Recently, using the Global Wavelet Analysis (also considering the Fourier Power Spectrum) the power spectra of the 3 GHz signal, observed at low (0.6 s) temporal resolution, have been determined (Rosa et al., 2002a,b). The 3 GHz radio burst power spectrum exhibits a power-law $\omega^{-\alpha}$ with $1.50 \leqslant \alpha \leqslant 1.82$ which is an evidence of stochastic process due to a self-affine dynamics as found in the MHD turbulence theory. The basic definition of a self-affine stochastic process is that the power spectral density of the corresponding time series has a power-law dependence on frequency and its correspondent time series can exhibit a finite correlation dimension due to anomalous fractal scaling over its Gaussian fluctuation (Theiler, 1991). The presence of this characteristic power-law implies that the fluctuations are correlated without a dominant characteristic time scale, as predicted in the models for multi-loop interactions (Tajima et al., 1987). From a previous analysis it follows that loop structures can exist in a broad range of

* Corresponding author. Tel.: +55 12 39456534; fax: +55 12 39456375.
E-mail address: reinaldo.rosa@pesquisador.cnpq.br (R.R. Rosa).

0273-1177/34.00 © 2007 COSPAR. Published by Elsevier Ltd. All rights reserved.
doi:10.1016/j.asr.2007.08.015

spatial scales and their mutual interactions give rise to the corresponding broad range of temporal scales with no preference for any particular period (Rosa et al., 2005).

An interesting aspect of these data, addressing its high resolution time series (0.01 s), is that the entire time series, as shown in Fig. 1, is composed by three impulsive clustered events (on the left, middle and right of the entire time series). The main profile, for each impulsive cluster, has a peak of low (<350 SFU), intermediate (350–500 SFU) and high amplitudes (>500 SFU). Of particular interest are the clustered events whose amplitudes range within relatively low solar flux units (<350 SFU), usually disregarded from statistical analysis due to their low amount of measurement points ($\ll 10^3$). As showed in Fig. 1 these events are interesting because their impulsive components are richer in fine structures than the more intense components (>500 SFU). As a consequence of this property the fine characterization of the underlying self-affine variability is less evident when compared to stochastic canonical fluctuation patterns as shown in Fig. 2a and b. For fluctuation patterns, showed in Fig. 2a and b, the power spectra are

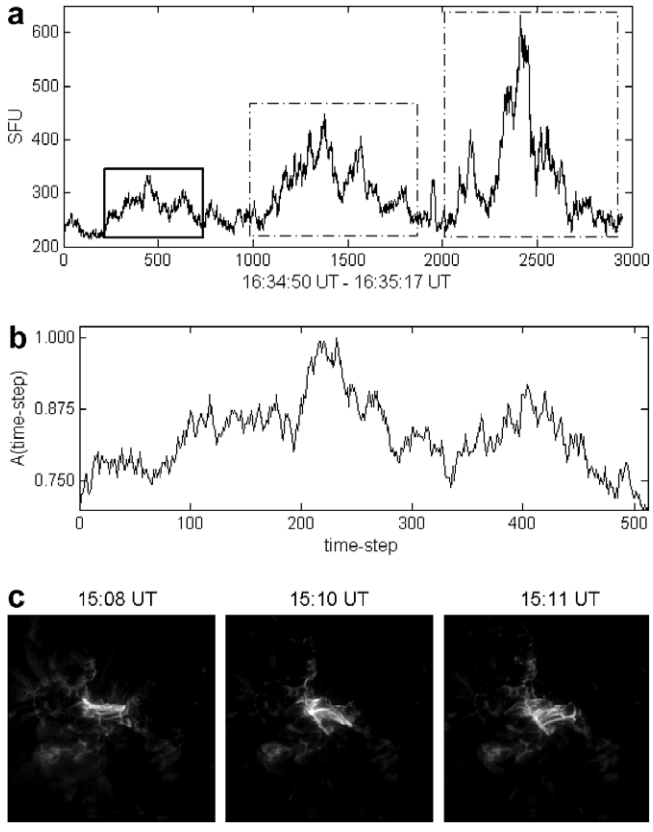

Fig. 1. (a) The corresponding time series for the 3.0 GHz solar radio flux observed, with 0.01 s resolution, from 16:34:50 to 16:35:17 UT in June 6, 2000 during a X2.3 solar flare. In the windows are impulsive clustered events where the peak is of low (<350 SFU), intermediate (350–500 SFU) and high amplitude (>500 SFU). In the small window on the left is shown a short weak clustered impulsive event composed by 512 time-steps. (b) The short weak clustered impulsive event with a normalized amplitude. (c) Selected snapshots, observed by TRACE (171 Å), representing the evolution of the complex mutual loop structure from where the X2.3 flare is observed.

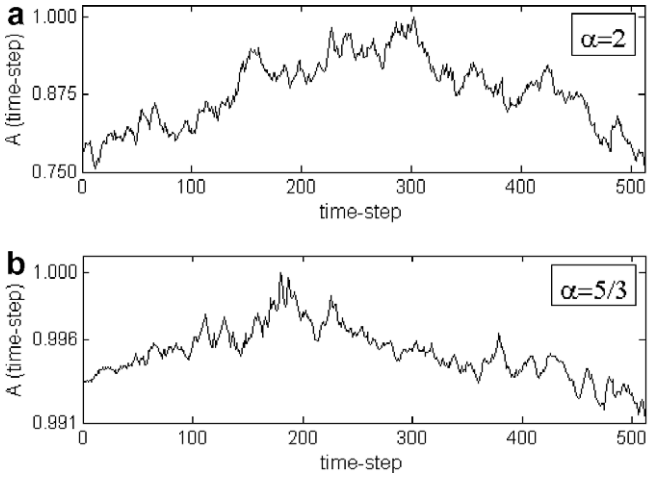

Fig. 2. (a) A fractional Brownian variability pattern; (b) A turbulent variability pattern. Both are short (512 points) and have an equivalent clustered impulsive profile pattern as the solar radio burst showed in Figure 1b.

also like $\omega^{-\alpha}$ with $\alpha = 2$ and $\alpha = 5/3$, respectively. These time series were generated with the same length of the selected short burst pattern showed in Fig. 2b (512 points) as the reference pattern variability for two slightly different canonical stochastic processes that will be introduced in Section 2.2. As mentioned above, the problem here is that time series like that are too short (($N < 10^3$ measurements) for robust power-law analysis aiming characterization of self-affine stochastic processes.

In this paper, a complementary analysis, for short non-stationary time series, is performed using the Gradient Pattern Analysis (GPA) (Assireu et al., 2002; Rosa et al., 2003) combined with the discrete wavelet decomposition (Percival and Walden, 2000; Bolzan, 2005). The asymmetry coefficient as a function of frequency provides a new kind of spectrum from where it is possible to classify the short temporal variability pattern taking into account a mutual information distance among particular gradient spectra. The proposal described here is to classify the selected short burst pattern variability (SBP) (Fig. 1b) estimating its mutual information distance with respect to the self-affine canonical patterns representing weak and strong MHD turbulent processes, respectively.

The paper is organized as follows: In the next Section we describe the data including the canonical simulated turbulent-like patterns. In Section 3 we introduce the gradient spectral analysis method and show the results from its application to the data described in Section 2. In the last Section we discuss the performance of the method in the context of solar physics.

2. Data

2.1. Selected solar burst

The June 6, 2000 flare, classified as X2.3, was observed during 15:00–17:00 UT in the active region NOAA AR

9026 (N21°, E23°). A full-halo coronal mass ejection and the type II radio burst were reported in association with this flare (Solar Flare NOAA Report). During the flare, two impulsive phases at 15:14–15:40 UT and 16:34–16:40 UT were observed by the Ondrejov radiospectrograph (Jiricka et al., 1993). The second phase of the flare was also observed by the EIT/SOHO and SXT/Yohkoh instruments (Rosa et al., 2005). Fig. 1a shows the main high resolution sample observed at 3 GHz in the interval of 16:34:50–16:35:17 UT with time resolution of 0.01 s (a time series composed of 2658 points) from where it is possible to select clustered impulsive bursts, specially those whose intensities are restricted to low solar flux units (<350 SFU). Fig. 1b shows the normalized selected short burst pattern (SBP) that has been analyzed in this paper. Due to its short composition it is impossible to characterize the robustness of the turbulent power-law, found by the whole burst, based uniquely in the global wavelet spectra of the SBP event. In Fig 1c are shown three snapshots, observed by TRACE (171 Å), representing the spatio-temporal dynamics of the complex mutual loop structure from where the X2.3 flare is observed.

2.2. Turbulent-like variability patterns

Stochastic intermittent fluctuations are characterized by time series that display multi-scaling, irregular and quasi-regular, amplitudes. Usually, intermittency is a characteristic of the underlying dynamics and it is difficult to quantify, as it appears in many variability patterns. A particularly relevant case for physics is when the energy spectrum of the stochastic intermittent fluctuations is a power-law compatible with turbulent process. In this context, one of the basic questions in the theory of MHD turbulence is on the slope of the one-dimensional energy spectra (Cho et al., 2002). Contrary to the hydrodynamic turbulence, the magneto-hydrodynamics (MHD) turbulence can exhibit a class of energy spectra $E(\kappa) \sim \kappa^{-\alpha}$ with $1 \leqslant \alpha \leqslant 7/3$ depending on the structural and dynamical aspects of the magnetic field and wave number, κ, involved. According to the traditional Iroshnikov–Kraichnan theory, the MHD turbulent spectrum has $\alpha = 3/2$ (Kraichnan, 1965). However, in this theory the MHD turbulence is formulated upon the assumption that the turbulent process is three-dimensionally isotropic and the nonlinearity becomes weaker at smaller scales describing only the weak turbulent process. In the last two decades analytic and high-resolution numerical simulations have shown that the MHD energy cascade is directed mostly perpendicularly to the guiding magnetic field, demonstrating that the MHD turbulent process is indeed anisotropic and, as the anisotropy is scale-dependent, eventually turbulence becomes strong (Mason et al., 2006). Anisotropic models for strong MHD turbulence where the process does not require intermittency have the form $E(\kappa_\perp) \sim \kappa_\perp^{-3/2}$ (Boldyrev, 2005). In the other hand, theoretical approaches for strong MHD turbulence considering intermittency affecting the scaling of higher-order correlation functions provide $E(\kappa_\perp) \sim \kappa_\perp^{-5/3}$ (Goldreich and Sridhar, 1995). Interestingly, intermittent anisotropic models forcing MHD weak turbulence have shown a power-law with $\alpha = 2$ (Galtier et al., 2002). In the present case, mutual interacting solar loop with nonlinear oscillations requires models considering both anisotropy (Fig. 1c) and intermittency (Fig. 1a and b). Thus, in the phenomenological analysis of the 3 GHz solar flare considering the scenario given in our previous papers (Rosa et al., 2002b, 2005), we investigate energy spectra from intermittent MHD turbulent-like stochastic variability patterns with $\alpha = 2$ (weak turbulence) and $\alpha = 5/3$ (strong turbulence).

In order to characterize the fluctuation pattern of the SBP time series, showed in Fig. 1b, we selected two turbulent-like variability patterns generated from the stochastic systems as given by Osborne and Provenzale (1989). In numerical theory of $1/\omega$ *noise* the spectrum of the stochastic process is sampled into a discrete series of frequencies and the random function is then computed as a discrete series at times $t_i = i\Delta t, i = 1, \ldots, M$. Thus, given a power spectrum of a random function $\omega_k, P(\omega_k) \sim \omega_k^{-\alpha}$, characterized by the spectral index α, they define the correspondent real random time series by simple superposition of harmonic oscillations given by

$$A(t_i) = \sum_{k=1}^{M/2} [P(\omega_k)\Delta\omega]^{1/2} \cos(\omega_k t_i + \phi_k), \quad i = 1, \ldots, M \tag{1}$$

where $\omega_k = k\Delta\omega$ ($k = 1, \ldots, M/2$), with $\Delta\omega = 2\pi/M\Delta t$, and the ϕ_k 's are the phases chosen to be random. The value of $M\Delta t$ is the length of the time series requiring that the spectrum has a high-frequency cutoff at the *Nyquist* frequency ($\pi/\Delta t$) (Panchev, 1971).

These stochastic time series have a self-affine structure in the increments and they represent a class of *fractional Brownian fluctuation of index* α with turbulent-like variability patterns. From the symmetry principles codified in group theory, self-affine fluctuations are only self-similar under specific scaling transformations (Barabási and Stanley, 1995). In that sense, fractional Brownian fluctuations are a generalization of ordinary Brownian motion, which corresponds to the case $\alpha = 1/2$ (Mandelbrot, 1999).

A remarkable aspect in this approach has been investigated by Rosa et al. (1998b) and Theiler (1991). They show that the correlation dimension for *fractional Brownian fluctuation* is a small finite value given by $\nu = 2/(\alpha - 1)$. From a phenomenological point of view, even for stochastic fluctuations driven by infinite modes as in turbulence, the space dimension where coherent structures arise is the relevant information given by distinct scaling regimes regulating the self-oscillatory dynamics.

Thus, although scaling can be observed as a universal characteristic, the causes of the scaling for different processes can be physically different. Two interesting cases are those involving turbulent fluids (neutral and ionized).

The case $\alpha = 2$ with $v = 2$ is for weak turbulence, where the turbulence is driven by 2D Lagrangian inhomogeneities without strong instabilities. As discussed above, this case is also valid for weak MHD turbulence as given by Galtier et al., 2002. The case $\alpha = 5/3$ with $v = 3$ is for strong turbulence driven by 3D Eulerian progressive fractionation of a three-dimensional structure due to strong instabilities, also valid for strong MHD turbulence with intermittency as given by the model of Goldreich and Sridhar, 1995. Actually, for fully developed turbulence we have $\alpha \approx 5/3$ in the inertial range and $\alpha \approx 2$ in the dissipative range (Yoshizawa et al., 2003).

As we are interested in the SBP profile, we first computed time series with 6000 points and then we selected SBP-like burst profiles composed of 512 points. Two examples were normalized, one for $\alpha = 2$ and the other for $\alpha = 5/3$, and they are shown in Fig. 2a and b, respectively.

3. The gradient spectral analysis

3.1. The asymmetry coefficient

Usually the characterization of irregular fluctuations from time series, as given by turbulent-like profiles, is performed on the amplitude differences, specifically on the kurtosis measures from the respective PDF. For that, it is necessary to have time series composed of $\sim 10^4$ points. For time series the GPA operation, described in the Appendix of this paper, is straightforward and brings some advantages on the traditional methodologies. The asymmetry coefficient G is intrinsically calculated on the amplitude differences (fluctuations) given by the gradient pattern. As the first gradient moment is very sensitive to small changes in the phase and modulus of each fluctuation vector, it can distinguish complex variability patterns even when they are very similar and consist of a low amount of vectors (Assireu et al., 2002).

The SBP profile under investigation in this paper is composed of only 512 SFU measurements. Thus, its respective matrix of fluctuations, in order to get the square correspondent minimum gradient lattice (22×22), must be constructed by taking 484 points. Note that 512 are not reducible to a square gradient lattice $L \times L$. This procedure can be conducted by taking the points from left to right or vice-versa, without loss of significant information (Assireu et al., 2002). Thus, from each 484 measurements, a value for G parameter is calculated from the operation on the respective square gradient lattice 22×22. Fig. 3 shows the 22×22 matrix of fluctuations for the first 484 measurements of the SBP profile shown in Fig. 1b.

All the signals considered in this analysis are rich in scales where the information about higher-order joint probability densities and self-affine dimensions are hidden. Thus, our second-step consists in obtaining the values of asymmetric coefficient for each inherent frequency of the signal. Thus, in such cases we can have the asymmetry coefficient as a function of frequency $G(\omega)$.

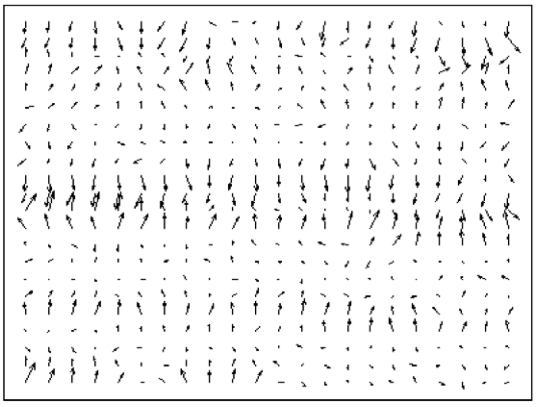

Fig. 3. The gradient pattern for the fluctuations among the first 484 measurements of the SBP profile showed in Figure 1b.

3.2. Wavelet decomposition

In a general framework, the wavelet transformation of a time series $A(t)$ is its deconvolution into a set of functions $\omega_{a,b}$ where $\omega_{a,\ b}(t) = a^{-1/2}\omega[a^{-1}(t-b)]$, all derived from the *mother wavelet* (MW) by translation b and scaling a (e.g., Farge, 1992; Torrence and Compo, 1998). The MW may be chosen to best reveal the signal's structure under consideration and, for very short time scale variability under nonlinear modulation, we choose the discrete Daubechies wavelet (DB8) (Daubechies, 1990). Thus, the wavelet decomposition of our time series was obtained following a dyadic scale, using one scale at each octave from 1 to 9, giving nine decompositions ($2^9 = 512$), where the frequencies are 1/2, 1/4, 1/8, 1/16, ..., 1/512 of the fundamental frequency, considered here as 1 Hz (for the normalized time series). Note that each original signal component provides a set of 9 specific 512 points time-series representing the typical scaling variability in that frequency. In Fig. 4a it is shown, as an example, the complete DB8 decomposition for the SBP time series. Once we have defined how to decompose each original time series in a set of nine scaling characteristic time series, the next step in our operation is to obtain the respective gradient spectra by computing the respective asymmetry coefficients.

3.3. Gradient spectra

For each set of decomposition it is possible to calculate the respective asymmetry coefficient G, so that for each signal it is possible to have the asymmetry coefficient as a function of the characteristic frequencies ω, $G(\omega)$. Thus, the gradient spectrum obtained from a N-measurements time series consists of ℓ values of G:$\{G(\omega_1), \ldots, G(\omega_\ell)\}$ where ℓ is the amount of discrete decomposed time series from the original signal, having $2^\ell = N$. In our case we have $\ell = 9$ and then the respective gradient spectrum $\{G(\omega_1), \ldots, G(\omega_9)\}$ can be plotted in the $G \times \log_{10}(\omega)$ space. Note that, instead of using the discrete dyadic decomposition, we could have a denser gradient spectrum

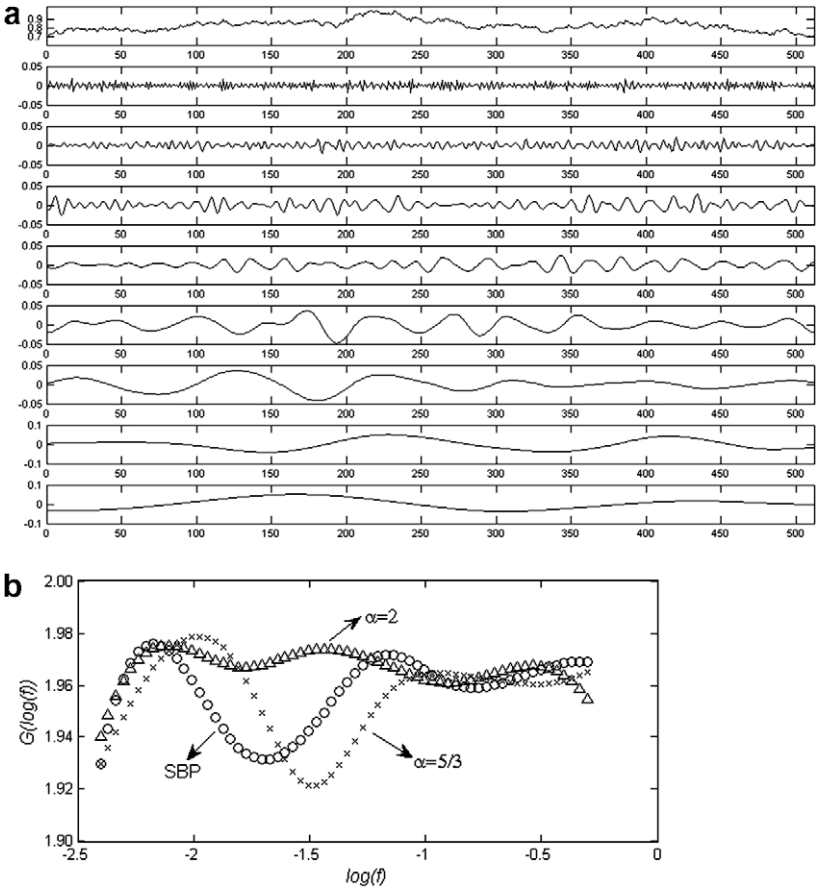

Fig. 4. (a) Db8 wavelet decomposition of the SBP time series. (b) The mutual gradient spectra obtained from the decomposition of each time series: solar burst (circle), turbulent (cross) and Brownian (triangle).

obtaining the equivalent continuous time–frequency domain by means of a continuous wavelet transform. Actually, from such continuous time–frequency domain, it would be possible to have an infinite set of time series and, consequently, a continuous gradient spectrum. However, based on the multiresolution analysis theory, it is easy to show that the reduction of the continuous wavelet transform to its equivalent discrete decomposition contains the main time–frequency components by means of the so-called asymptotic representation. Moreover, the signals are well approximated by a superposition of spectral lines that represent a smooth transition between each pair of frequency or period component guided by the wavelet skeleton (Mallat, 1989). Thus, for a given decomposed signal, the search for its best gradient spectrum is well performed by interpolating the ℓ points using a nonlinear fitting. After fitting the ℓ points by a cubic spline, we can resample the original ℓ points gradient spectrum by a denser set of points. This, of course, costs much less computationally than using a continuous wavelet transform to obtain the gradient spectrum and, for our analysis, the denser resample procedure is necessary to estimate, with high precision, the normalized mutual information distance between a pair of gradient spectra.

3.4. The normalized mutual information distance

Based on the concept of relative entropy (or Kullback–Leibler distance) (Kullback and Leibler, 1951), the normalized mutual information distance, δ_N, is defined here as

$$\delta_N(\chi/\rho) = \frac{1}{N}\sum_{n=1}^{N}\chi_n \ln\left(\frac{\chi_n}{\rho_n}\right) \tag{2}$$

where ρ_n is the reference discrete gradient spectrum (in this paper, it is alternatively the gradient spectra for one of the canonical time series) and χ_n is the discrete gradient spectrum to be characterized (in this paper, it is the gradient spectrum for the SBP time series). It is easy to show that δ_N converges when the total number of gradient spectral points is $N \geqslant 10^2$, so that we always use this criterion in our denser discrete resample from the fitted continuous function. For the time series analyzed in this paper, the relative entropic distances, δ_N, have been calculated considering at least 16 interpolated points between each two adjacent points of the original gradient spectrum. Thus, we have computed the normalized mutual information distances between gradient spectra having, at least,

$8 \times 16 = 128$ spectral points each, satisfying the convergence condition mentioned above.

In Fig. 4b we can appreciate each characteristic gradient spectrum: weak turbulence (Δ), strong turbulence ($\times$) and SBP (o). The values of δ_N obtained having χ_n as the SBP are $\delta_N(\chi|\rho_{\alpha=2}) = 0.061 \pm 0.002$ and $\delta_N(\chi|\rho_{\alpha=5/3}) = 0.016 \pm 0.002$. Thus, comparing these values for δ_N, we found the SBP closer to the strong MHD turbulent-like pattern variability.

Performing several calculations ($\sim$200) for distinct groups of short stochastic *fluctuations*, especially for both MHD turbulent phenomenologies ($\alpha = 2$ and $\alpha = 5/3$), we obtained a mutual information distance of 0.08 ± 0.01 between their respective gradient spectra.

4. Concluding remarks

Previous analysis of the 3 GHz radio burst investigated in this work has shown the presence of a power-law $\omega^{-\alpha}$ with $1.50 \leqslant \alpha \leqslant 1.82$, which is an evidence of a stochastic self-affine dynamics, probably related to the nonlinear loop structure interactions in the solar corona. In this paper, we have shown a more precise characterization of the weaker component of this burst (here we call SBP) found in the low amplitude clustered impulsive event with intensity <350 SFU. Our analysis, based on an innovative methodology called *gradient spectral analysis*, has been classifying the time variability profile of this SBP burst component as a strong MHD turbulent-like pattern, a process with spectral index $\alpha = 5/3$ (Goldreich and Sridhar, 1995). In the other hand, some theoretical approaches for solar radio emission are based on plasma instabilities and Langmuir turbulence without the explicit power-law derivation (e.g., Rizzato et al., 2003). Therefore, understanding of turbulent-like variability patterns is a necessary requirement for making further progress in the 1–3 GHz solar flare radio emission interpretation.

In order to understand the role of plasma turbulence in the development of solar flares, this result suggest that anisotropic strong MHD intermittent turbulent process can play a fundamental role in the generation of solar bursts observed in the 1–3 GHz range. In that sense, scaling free processes as intermittency and coherent states driving the loop system MHD coalescence instabilities can be considered in the interpretation of complex solar radio bursts and their EUV spatio-temporal counterpart (e.g. Aschwanden et al., 2001).

Considering the correspondent correlation dimension $\nu = 3$ and more intense and long radio bursts, attention should also be given to other MHD 3D processes, such as formation of MHD dissipative structures from a progressive fragmentation of a three-dimensional structure and scale-dependent dynamics alignment (Mason et al., 2006).

As a final note, it is expected that the analysis presented here will prove useful in investigations of short complex bursts belonging to solar flare radio signature and the addition of statistical significance tests will improve both quantitative and qualitative phenomenology of gradient spectral analysis. In a general perspective, we believe that the gradient spectra can be applied to proceed a fine phenomenological classification of the time variability patterns of many radio bursts (types I, II, III, pulsations, etc) observed in dynamical spectra.

Acknowledgment

The authors acknowledge the financial support from FAPESP and CNPq and the referees for valuable suggestions.

Appendix A. The Gradient Pattern Analysis

The Gradient Pattern Analysis (GPA) (Rosa et al., 1998a,b, 1999, 2000, 2003; Ramos et al., 2000; Assireu et al., 2002; Baroni et al., 2006a) is an innovative technique, which characterizes extended patterns based on large and small amplitude fluctuations of the spatial, temporal, and spatio-temporal structures represented as a static or dynamical gradient lattice. The local fluctuation between each pair of amplitudes of the global pattern is characterized by its gradient vector at corresponding mesh-points in the two-dimensional space. In this representation, the relative values between adjacent amplitudes (“local fluctuations”) are relevant, rather than the respective absolute values.

Note that in a gradient field such relative values can be characterized by each local vector norm and its orientation (phase). In this approach, each local fluctuation is represented by a vector in a 2d-space. Thus, according to Rosa et al. (2003), a given scalar field of fluctuations can be represented as a composition of four gradient moments: g_1, the integral representation of the fluctuation distribution (vectors); g_2, the integral representation of the corresponding norms; g_3, the integral representation of corresponding phases; and g_4, the complex representation of the gradient pattern (a complex coefficient composed by each corresponding pair of norm and phase). Considering the sets of local norms and phases as discrete compact groups, spatially distributed in a square lattice, the gradient moments have the basic property of being globally invariant (for rotation and modulation).

In this paper we use the first gradient moment, similarly as given by Assireu et al. (2002), which we are identifying here as the asymmetry coefficient G. For a given $L \times L$ global fluctuation pattern the coefficient G can be computed by means of the asymmetric amplitude fragmentation (AAF) operator (Rosa et al., 1999). This computational operator measures the symmetry breaking of a given fluctuation lattice and has been used in several characterizations (e.g., daSilva et al., 2000; Neto et al., 2001; Rosa et al., 2003; Baroni et al., 2006b).

Thus, the gradient measurement of asymmetric fluctuation, called here *asymmetry coefficient G*, is given by

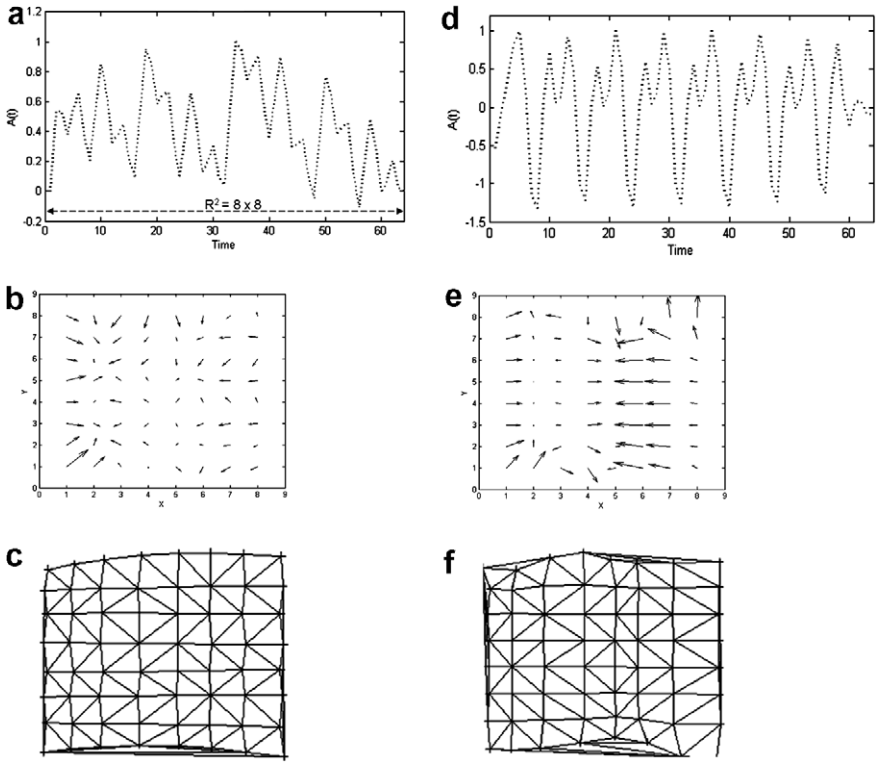

Fig. A.1. GPA of two examples of time series composed by 64 points each (a and d). The respective gradient lattices (b and e) and triangulation fields (c and f).

$G = |\varepsilon - f|/f$, where f is the number of asymmetric fluctuations and ε is the geometric energy correlation given by the number of connections among all fluctuations. The geometric connection among the fluctuations is generated by a Delaunay triangulation, taking the middle points of the asymmetric fluctuations as vertices. Due to the possible changes in the phases of each fluctuation (a vector in the gradient lattice), the parameter ε is very sensitive in detecting local asymmetric fluctuations on the gradient lattice (Rosa et al., 1999). Several calculations on random patterns have shown that the parameter G quantifies the level of asymmetric fluctuations and it is much more sensitive and precise in characterizing irregular fluctuations than the correlation length measures (Rosa et al., 1999). When there is no asymmetric correlation in the fluctuation pattern, the total number of asymmetric vectors is zero and then, by definition, G is null. For a random and totally disordered fluctuation pattern, G has the highest value. For a complex pattern composed by locally asymmetric fluctuations, G is nonzero, defining different classes of irregular fluctuation patterns. Fig. A.1 shows the GPA applied on two examples of short time series composed of only 64 points each (A.1a and A.1d). In Fig. A.1b and A1e the respective gradient lattices are shown. Fig. A.1c and A.1f show the respective triangulation fields (A.1c and A.1f). The examples are multi-periodic signals generated by arbitrary sine function summations. Note that for more regular and low frequency fluctuations the triangulation field captures an increase of regularity in the gradient lattice.

References

Aschwanden, M.J., Schrijver, C.J., Alexander, D. Modeling of coronal EUV loops observed with TRACE. I. Hydrostatic solutions with nonuniform heating. Astrophys. J. 550, 1036, 2001.

Assireu, A.T., Rosa, R.R., Vijaykumar, N.L., Lorenzetti, J.A., Rempel, E.L., Ramos, F.M., Abreu Sá, L.D., Bolzan, M.J.A., Zanandrea, A. Gradient pattern analysis of short nonstationary time series: an application. Physica D 168 (1), 397–403, 2002.

Barabási, A.-L., Stanley, H.E. Fractal Concepts in Surface Growth, Cambridge, 1995.

Baroni, M.P.M.A., Rosa, R.R., Silva, A.F., Pepe, I., Roman, L.S., Ramos, F.M., Ahuja, R., Persson, C., Veje, E. Modeling and gradient pattern analysis of irregular SFM structures of porous silicon. Microelectr. J. 37, 290–294, 2006a.

Baroni, M.P.M.A., Conceição, M.V., Rosa, R.R., Persson, C., Arwin, H., Silva Jr., E.F., Roman, L.S., Nakamura, O., Pepe, I., Silva, A.F. Optical, thermal and structural properties of porous diamond-like-carbon films deposited by magnetron sputtering. J. Non-Cryst. Solids 352, 3734–3738, 2006b.

Boldyrev, S. On the spectrum of magnetohydrodynamic turbulence. Astrophys. J. 626, L37–L40, 2005.

Bolzan, M.J.A. Statistical and wavelet analysis of the solar wind data. Braz. J. Phys. 35 (3A), 592–596, 2005.

daSilva, A.F., Rosa, R.R., Roman, L.S., Veje, E., Pepe, I. Characterization of asymmetric fragmentation patterns in SFM images of porous silicon. Solid State Commun. 113, 703–707, 2000.

Cho, J., Lazarian, A., Vishniac, E.T. Simulations of MHD turbulence in a strongly magnetized medium. Astrophys. J. 564, 291–301, 2002.

Daubechies, I. The wavelet transform, time-frequency localization and signal analysis. IEEE Trans. Inform. Theory 36, 961–1004, 1990.

Farge, M. Wavelet transforms and their applications to turbulence. Ann. Rev. Fluid Mech. 24, 394–457, 1992.

Galtier, S., Nazareno, S.V., Newell, A.C., Pouquet, A. Anisotropic turbulence of shear-alfvén waves. Astrophys. J. 564, L49–L52, 2002.

Goldreich, P., Sridhar, S. Toward a theory of interstellar turbulence. 2: Strong alfvenic turbulence. Astrophys. J. 438, 763–775, 1995.

Jiricka, K., Karlicky, M., Kepka, O., Tlamicha, A. Fast drift burst observations with the new Ondrejov radiospectrograph. Sol. Phys. 147, 203–208, 1993.

Kraichnan, R.H. Lagrangian-history closure approximation for turbulence. Phys. Fluids 8, 1385, 1965.

Kullback, S., Leibler, R.A. On information and sufficiency. Ann. Math. Stat. 22 (1), 79–86, 1951.

Kuperus, M. The role of plasma turbulence in the development of solar flares. Sol. Phys. 47 (1), 79–90, 1976.

Mallat, S. A theory for multiresolution signal decomposition: the wavelet representation. IEEE Trans. Pattern Anal. Mach. Intell. 11, 674–693, 1989.

Mandelbrot, B.B. 1/F Noise: Wild Self-Affinity in Physics. Springer-Verlag, 1999.

Osborne, A.R., Provenzale, A. Finite correlation dimension for stochastic systems with power-law spectra. Physica D 35, 357–381, 1989.

Panchev, S. Random Functions and Turbulence. Pergamon, Oxford, 1971.

Percival, D., Walden, A., Wavelets Methods for Time Series Analysis, Cambridge, 2000.

Ramos, F.M., Rosa, R.R., Neto, C.R., Zanandrea, A. Generalized complex entropic form for gradient pattern analysis of spatio-temporal dynamics. Physica A 283, 171–174, 2000.

Rizzato, F.B., Chian, A.C.-L., Alves, M.V., Erichsen, R., Lopes, S.R., de Oliveira, G.I., Pakter, R., Rempel, E.L. Langmuir turbulence and solar radio bursts. Space Sci. Rev. 107 (1-2), 507–514, 2003.

Mason, J., Cattaneo, F., Boldyrev, S. Dynamic alignment in driven magnetohydrodynamic turbulence. Phys. Rev. Lett. 97, 255002, 2006.

Neto, C.R., Rosa, R.R., Ramos, F.M. Multiscale analysis from turbulent time series with wavelet transform. Int. J. Mod. Phys. C 12 (8), 1261–1269, 2001.

Rosa, R.R., Sharma, A.S., Valdivia, J.A., Sawant, H.S. Characterization of localized turbulence in plasma extended systems. Physica A 257, 509–514, 1998a.

Rosa, R.R., Neto, C.R., Ramos, F.M., Sharma, A.S., Valdivia, J.A., Computational operators for dynamical complex patterns recognition. European Physical Society (Ed.), EPS-modeling Collective Phenomena in Complex Systems, 22F, pp. 304–305. 1998b.

Rosa, R.R., Sharma, A.S., Valdivia, J.A. Characterization of asymmetric fragmentation patterns in spatially extended systems. Int. J. Mod. Phys. C 10, 147–163, 1999.

Rosa, R.R., Pontes, J., Christov, Ramos, F.M., Neto, C.R., Walgraef, D. Gradient pattern analysis of Swift-Hohenberg dynamics: phase disorder characterization. Physica A 283, 156–159, 2000.

Rosa, R.R., Vats, H.O., Ramos, F.M., Zanandrea, A., Neto, C.R., Fernandes, F.C.R., Vijaykumar, N.L., Sawant, H. Characterization of local self-similarity and criticality in the solar active regions. Adv. Space Res. 29 (3), 463–466, 2002a.

Rosa, R.R., Ramos, F.M., Sawant, H.S., Fernandes, F.C.R., Vijaykumar, N.L., Zanandrea, A., Karlicky, M. Radio signature of multi-scaling flare loop interactions. in: Proc. 10th Eur. Solar Phys. Meet., ESA SP-506, pp. 737–740, 2002b.

Rosa, R.R., Campos, M.R., Ramos, F.M., Fujiwara, S., Sato, T. Gradient pattern analysis of structural dynamics: application to molecular system relaxation. Braz. J. Phys. 33, 605–609, 2003.

Rosa, R.R.; Karlick, M.; Zanandrea, A.; Sych, R.A.; Sawant, H.S.; Krishan. Characterization of solar multi-scaling magnetic loop interactions. AIP Conference Proceedings 784 (2), 567–573, 2005.

Tajima, T., Sakai, J., Nakajima, N., Kosugi, T., Brunel, F., Kundu, M.R. Current loop coalescence model of solar flares. Astrophys. J. 321, 1031, 1987.

Theiler, J. Some comments on the correlation dimension of 1/f noise. Phys. Lett. A 155 (8,9), 480–493, 1991.

Torrence, C., Compo, G.P. A practical guide to wavelet analysis. Bull. Am. Meteorolog. Soc. 79 (1), 61–78, 1998.

Yoshizawa, A., Itoh, S.I., Itoh, K. Plasma and Fluid Turbulence: Theory and Modelling. Institute of Physics Publishing, Bristol, 2003.